ISSN 2314-5609
Nuclear Sciences Scientific Journal
13, 152-181
2024
https://nssi.journals.ekb.eg

GEOCHEMISTRY, PETROGRAPHY AND RADIOACTIVITY OUTLINE OF HAMRAT AL-JIRJAB GRANITIC PLUTON, ESH EL MELLAHA RANGE, NORTH EASTERN DESERT, EGYPT

By

Mahmoud M. Badran, Sameh Z. Tawfik, Hussien. K. El Den, Wael M. El Maadawy, Ibrahim B. Abd El Kader and Amal S. Nasr.

Nuclear Materials Authority

ABSTRACT

Esh El Mellaha range is an uplifted block that is located in the North Eastern Desert of Egypt. It is the western extension of the Arab-Nubian Shield. It occurs as an elongated ridge parallel to the Gulf of Suez in the NW-SE direction. Gabal (G.) Hamrat Al-Jirjab crops out in the form of elliptical younger granitic pluton and considered as post-orogenic granite. It is an alkali feldspar granite type originated from peraluminous Calc-alkaline highly fractionated magma. This magma is rich in Rb but lake in Ba which reflects low pressure conditions. It was intruded at crustal depth greater than 20km at water pressure between 1 and 3 Kb. It was crystallized at temperatures ranging from 800 to 850°C.

The alkali feldspar granites of Hamrat Al-Jirjab pluton is uraniferous granites originated from highly fractionated U-rich magma. They show high U and Th contents and low Th/U ratio due to high concentrations of U in the accessory minerals (Zircon, apatite, sphene and fluorite).

The studying samples were investigated by using NaI(Tl) detector to evaluate the radiological hazards and compare them with the world average values. The average activity concentrations for ^{238}U,^{232}Th, ^{226}Ra and ^{40}K with an average value of (208.2), (138.6), (115,8), (1091.9) respectively. The obtained values were higher than the recommended values. Radiological hazard parameters were estimated based on the activity concentrations of ^{238}U, ^{232}Th, ^{226}Ra and ^{40}K and compared with the internationally approved values and the recommended safety limit.

Keywords: Hamrat Al-Jirjab, Esh El Mellaha, North Eastern Desert, Geochemistry, Radioactivity

1. INTRODUCTION

Gabal (G.) Hamrat Al-Jirjab is delineated by latitudes 27° 44' and 27° 48'N and by longitudes 33° 17' and 33° 22' 33"E (Fig. 1). It covers an area of about 10 Km^2 forming conspicuous reddish white topographic land mark with moderate relief nearly 433 m a.s.l. (above sea level). It is dissected by Wadi Abu Masannah into two main parts (northern and southern).

The study area can be reached through Cairo-Hurghada asphaltic road along the Red Sea coast, nearly 383 Km from Cairo, then turn west through the old asphaltic road for about 15 Km to reach Esh El Mellaha range.

Fig. (1): Location map of G. Hamret Al-Jirijab, Esh El Mellaha range, North Eastern Desert, Egypt

2. FIELD INVESTIGATIONS

The geologic map of the area (after Abd El Baset, 2013) shows the distribution of rock units and their field relations (Fig. 2). The main rock units exposed at Hamrat Al-Jirjab area are chronologically arranged from oldest to youngest as:

Post granitic dykes (**youngest**)

Alkali feldspar granites

Dokhan volcanics (**oldest**)

2.1. Dokhan volcanics

Dokhan volcanics are the oldest rocks at Hamrat Al-Jirjab that are cropping out as hard, massive dark grey to greenish grey and purple to black hills of moderate to high peaks. They reach 448 m (a.s.l.) and spread in both northern and southern parts of G. Hamrat Al-Jirjab. They are cut by the alkali feldspar granites with sharp intrusive contact and sometimes receiving offshoots and veinlets of the alkali feldspar granites. The Dokhan volcanics are overlained unconformably by

Phanerozoic sediments. They are extruded by post granitic dykes of acidic, intermediate and basic varieties as well as quartz veins (Bentor, 1985; Kröner, 1984; Stern and Hedge, 1985 and Shackleton, 1986).

2.2. Alkali feldspar granits

Alkalifeldspar granites are well represented by Hamrat Al-Jirjab younger granites they cover an area of about 10 Km^2. They have semi-circular shape and show rugged relief with moderate to high peaks reaching 433 m (a.s.l.). The alkali feldspar granites are medium to coarse-grained with reddish pink to red color.

They are hard and blocky but some parts are highly weathered forming rounded to sub-rounded cavities of different diameters. Kaolinitization, chloritization and hematitization are the main detected alteration features of the alkali feldspar granites. They are dissected by few numbers of dykes of different composition and also affected by faults and shear zones. Joints and fault planes are stained with reddish brown to brick red solutions. They have some pegmatitic pockets and aplite veins and also traversed by quartz veins in various directions. The exfoliation structure is noticeable along the marginal slopes as a result of load release effect.

2.3. Post granitic dykes

The post granitic dykes cut through the Dokhan volcanics and the alkali feldspar granites with few numbers in various directions. They range in thickness from 0.5 to 10 m and extend for several kilometers. They can be classified according to their composition into acidic, intermediate and basic dykes (Figs. 3-a, b, and c).

2.3.1. Acidic dykes

They are represented by granophyre, felsite and aplite, granophyres and felsites dykes are fine-grained, massive, hard and exhibiting different colors ranging from red, reddish pink, buff to pale brown. They have sharp contacts with the enclosing rocks since they are more resistant to erosion than the country rocks. They vary in width from half a meter to several meters trending mainly ENE-WSW, NE-SW, WNW-ESE and NW-SE.

The aplite dykes are microgranites easily distinguished by their sugary structure. They are pinkish white in color trending mainly E-W and NW-SE. They extend for tens of meters with thickness varying from 5 to 20 Cm. (Fig. 3-a).

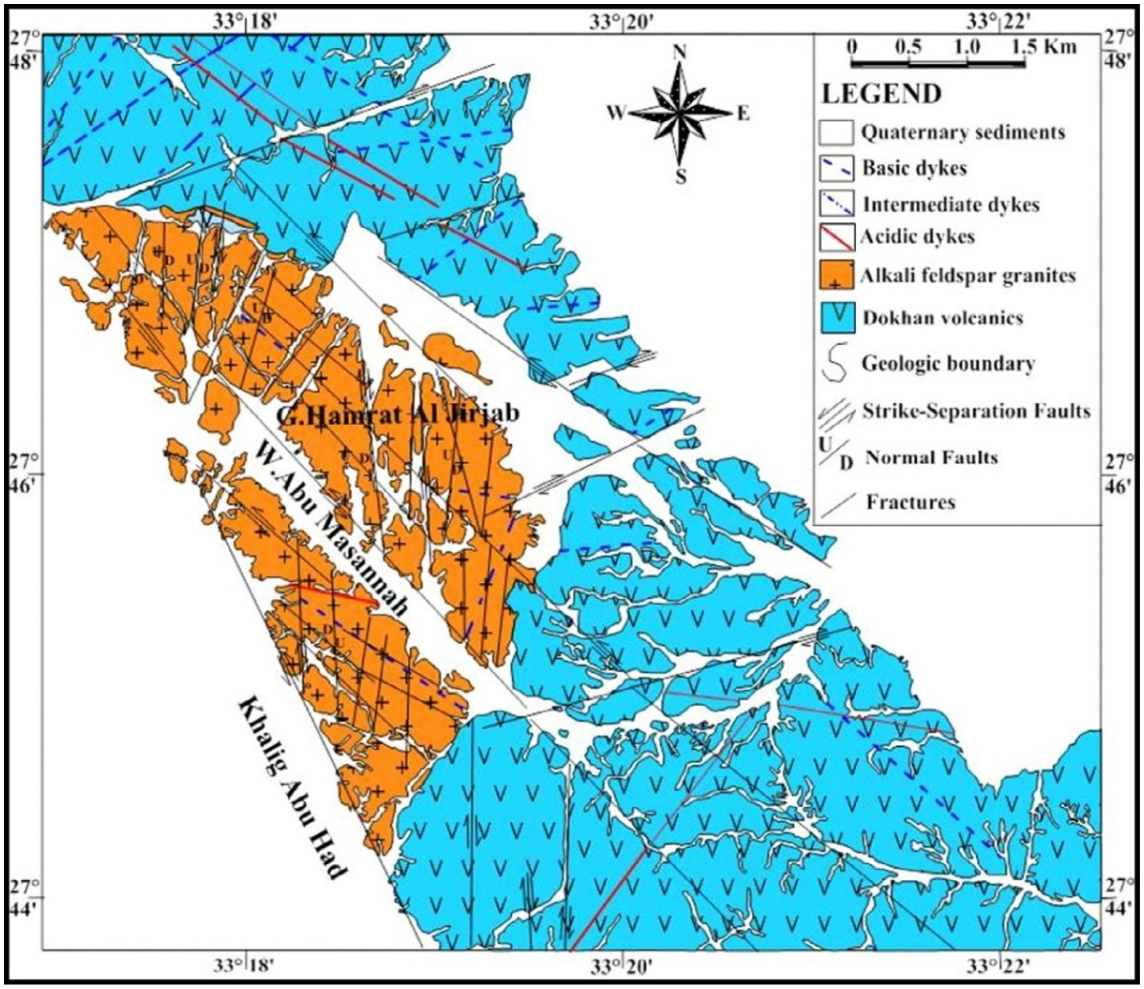

Fig. (2): Geological map of Hamrat Al-Jirjab area, Esh El Mellaha range, North Eastern Desert, Egypt (after Abd El Baset, 2013)

2.3.1. Intermediate dykes

This type of dykes is few with limited distribution. They are mainly fine- to medium-grained andesites. They are hard and massive with greyish green to brownish green color with porphyritic texture of plagioclase laths imbedded in fine-grained matrix. They run mainly in the NE-SW direction (Fig. 3-b).

2.3.1. Basic dykes

They are the youngest and most abundant set of dykes in Hamrat Al-Jirjab granitic intrusion. They are doleritic in composition, fine-grained with pale green to dark greenish grey color. They are relatively less resistant to weathering than their host rocks and occasionally leave deep elongated trenches. They are straight to slightly curved with long extensions and vary in their thickness along their strike and trending generally NE-SW (Fig. 3-c).

2.4. Structure of Hamret Al-Jirjab intrusion

Hamrat Al-Jirjab intrusion is divided by a major fault trending NW-SE into northern and southern masses. The two parts are strongly traversed by faults and joints. Joints are mostly of the tensions type with long extensions. The

recorded fault zones are strike-slip separation and normal faults associated with silicification, hematitization, kaolinitization, brecciation and slickenside.

The NW-SE and N-S fault directions are the most dominant trends. Figure (4) shows the rose diagram constructed on the basis of fault number and length showing the main fault trends. Salman et al., (1995) stated that the N-S trend is the youngest among the fault trends in the area.

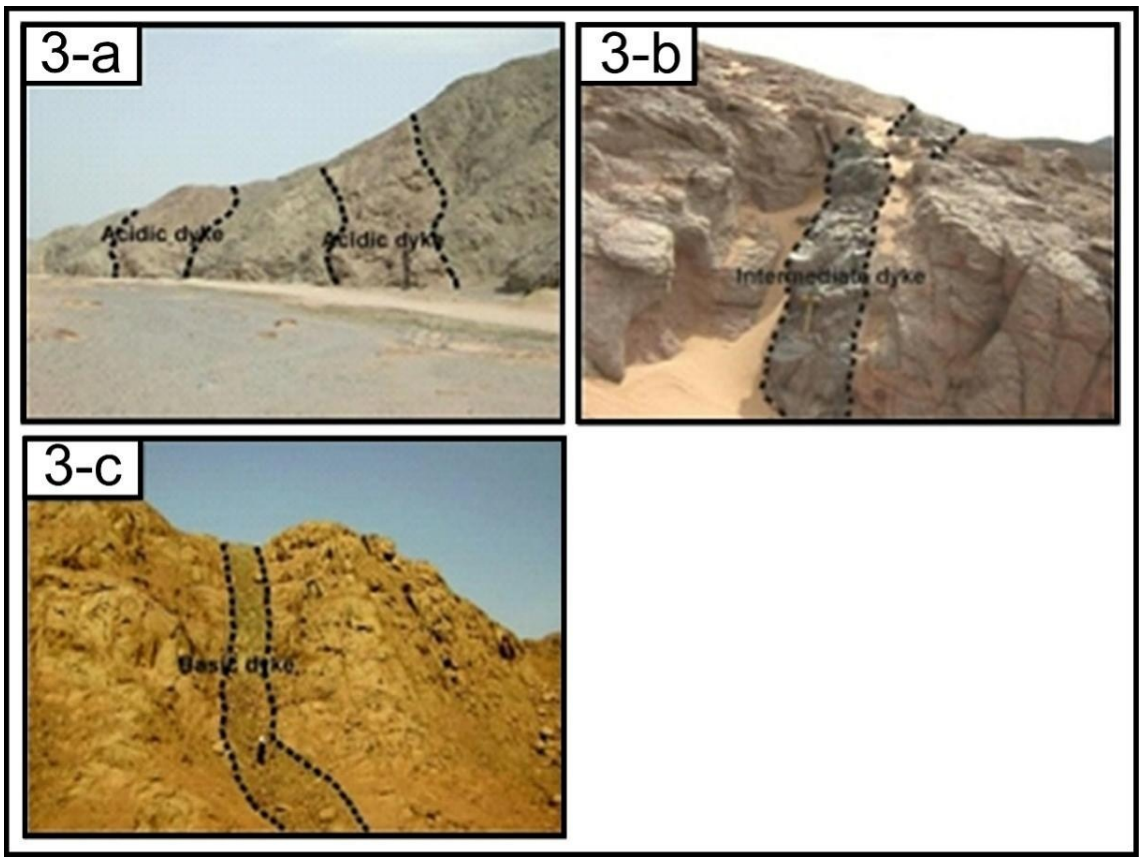

Fig. (3-a): Acidic dykes dissecting the Dokhan volcanics of Hamrat Al-Jirjab area, looking. NW

Fig. (3-b): Intermediate dyke dissecting the alkali feldspar granites of Hamrat Al-Jirjab area, looking W.

Fig. (3-c): Basic dyke dissecting the alkali feldspar granites of Hamrat Al-Jirjab area, looking S

The joints of Hamrat Al-Jirjab intrusion are well developed striking in various directions with different scales. Some are filled with quartz, aplite and pegmatite veinlets with iron and magnesium oxides. The WNW-ESE, E-W, NW-SE and N-S directions are the main trends for these joints arranged in descending order.

3. PETROGRAPHIC STUDIES

Elven represented samples are used to petrographic study of the Dokhan volcanics and alkali feldspar granites. Eight representative samples

from alkali feldspar granites were selected for modal analysis and were plotted on the QAP ternary diagram of Streckeisen (1976). It is clear that Hamrat Al-Jirjab younger granite samples plot in the alkali feldspar granites field (Fig. 5). Table (1) shows the modal analyses for the studied younger granites of Hamrat Al-Jirjab intrusion.

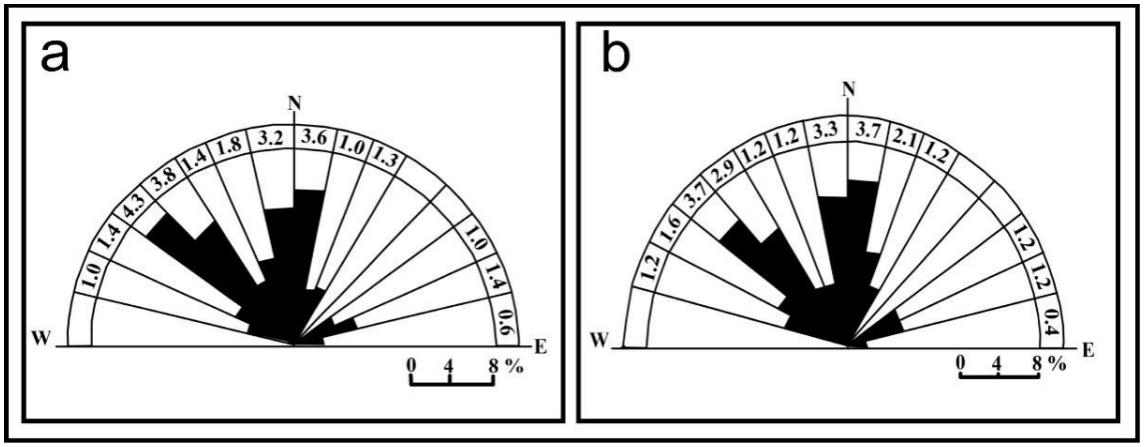

Fig. (4): Rose diagram of fault lines in length proportion (a) and number proportion (b), Hamrat Al-Jirjab area, after Salman et. al., 1995.

Table (1): The modal analysis of the studied younger granites.

Rock Type	No.	Mineral composition					
		Quartz	Perthites	Plagioclase	Mica	Hornblende	Accessories opaques
Alkali feldspar granite	1	32.95	60.55	3.00	2.50	-	1.00
	2	33.15	58.00	3.65	2.00	-	3.20
	3	27.87	66.45	2.10	2.15	-	1.43
	4	25.97	70.26	1.65	1.11	-	1.00
	5	29.28	65.71	2.10	1.85	-	1.06
	6	31.45	59.05	4.50	3.87	-	1.13
	7	29.73	63.47	4.35	1.40	-	1.05
	8	30.11	61.59	4.55	2.50	-	1.25

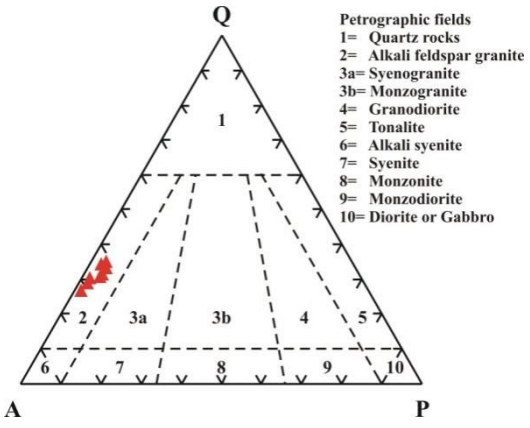

Fig. (5): Modal composition for the studied granites (after Streckeisen, 1976)

3.1. Dokhan volcanics

Dokhan volcanics in the study area can be classified as lava flows as well as their pyroclastic. Lava flows, in the study area, could be subdivided into intermediate and acidic varieties. The intermediate Dokhan volcanics are represented by andesite, while the acidic varieties are mainly represented by dacite. These lava flows exhibit different textures characterizing the stages of the lava flows.

3.1.1. Intemediate Dokhan volcanics

Intermediate Dokhan Volcanics are mainly represented by andesite. They are commonly porphyritic and composed of abundant plagioclase and hornblende phenocrysts embedded in a fine-grained groundmass of the same composition. The main accessory minerals are apatite and iron oxides while chlorite, epidote and saussurite are secondary minerals. Plagioclase (An_{34-37}) occasionally appears as elongated subhedral to euhedral phenocrysts ranging from 0.3 to 3.5 mm in length. They are generally arranged in subparallel orientation, suggesting flow texture. Plagioclase occasionally appears as elongated crystals with characteristic simple and lamellar twinning (Fig. 6a). They are partially altered to saussurite, chlorite and epidote, especially along cores and cleavage planes. Some crystals are highly cracked and sometimes these cracks are filled with the groundmass minerals.

Hornblende occurs as subhedral to euhedral prismatic phenocrysts ranging from 0.3 to 2.5 mm in length. They are strongly pleochroic from pale to dark green.

The accessory and secondary minerals represent minor amounts of the total volume. They occur as disseminations and clusters within and/or between other crystals. They are represented by quartz, iron oxides and apatite with chlorite, saussurite and epidote as alteration products. Apatite occurs as euhedral to subhedral prismatic crystals (Fig. 6b).

3.1.2. Acidic Dokhan volcanics

Acidic Dokhan volcanics are mainly represented by dacite. These rocks are mainly composed of plagioclase, biotite, quartz and potash feldspars as well as few hornblende crystals embedded in a micro-to cryptocrystalline groundmass composed of small lathes of plagioclase, quartz, biotite, chlorite, and epidote. Zircon and iron oxides are found as accessory minerals. This rock type is sometimes fractured; the fractures are filled with secondary muscovite and quartz. Plagioclase (An_{24-28}) occurs as subhedral to anhedral oligoclase phenocrysts showing lamellar twinning. They are partially altered to saussurite.

Quartz is common in the groundmass rather than phenocrysts. It occurs as crystals surrounding the plagioclase and other minerals (Fig. 6c). Potash feldspars are found as subhedral tabular crystals of sanidine (Fig. 6d),

Biotite occurs as subhedral to euhedral flakes of light brown color and is highly altered to chlorite especially along peripheries and cleavage planes.

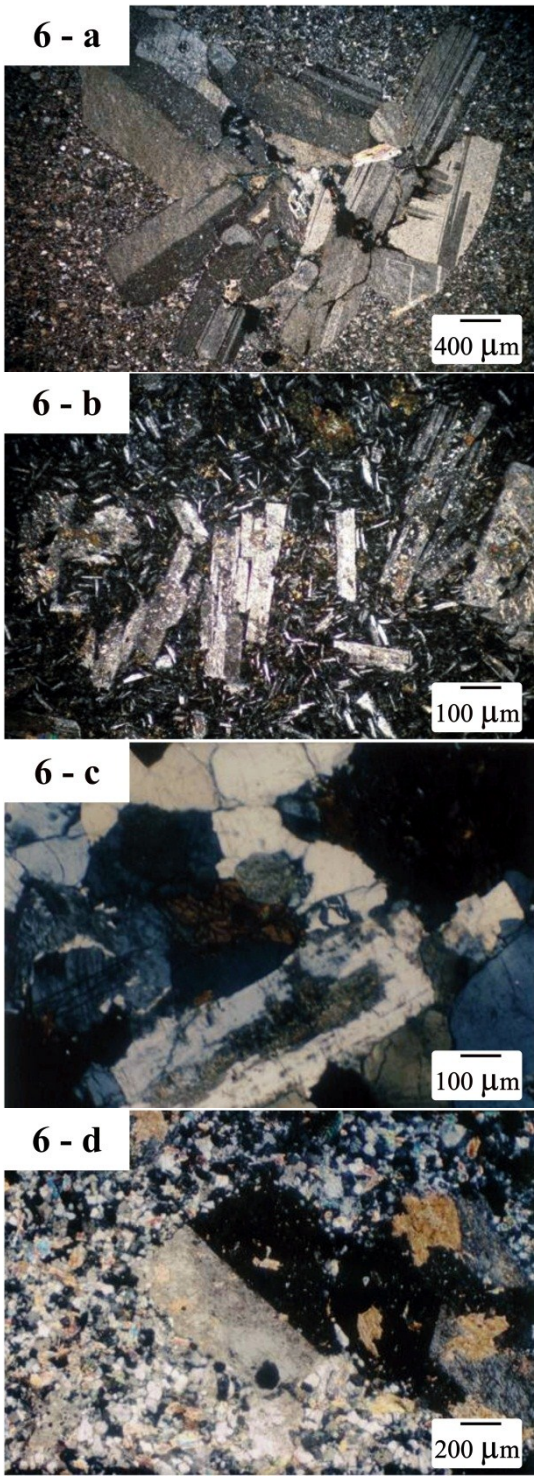

Fig. (6-a): Lamellar twinning of plagioclase phenocryst in porphyritic andesite, C.N.
Fig. (6-b): Euhedral to subhedral prismatic apatite crystal in porphyritic andesite, C.N.
Fig. (6-c): Plagioclase phenocryst associated with quartz in dacite, C.N.
Fig. (6-d): Subhedral tabular of sanidine crystal as potash feldspar in dacite, C.N.

3.2. Alkali feldspar granite

In hand specimen, the alkali feldspar granites of Hamrat Al-Jirjab area are medium to coarse-grained, leucocratic with pink to reddish pink in color. Under the microscope, these rocks are holocrystalline, equigranular and essentially composed of potash feldspars and quartz with small amounts of plagioclase. Biotite and muscovite occur in subordinate amounts. Chlorite and sericite are the secondary minerals as alteration products. Zircon, fluorite, allanite, and iron oxides are the main accessory minerals.

Potash feldspars are fairly abundant forming (48.5-54.1%) of the modal composition (Table 1) and mainly represented by feather and string perthite (Fig. 7a). They occur as subhedral to anhedral crystals of orthoclase perthite. Perthite is observed as subhedral crystals (Fig. 7b).

Sometimes, perthite crystals poikilitically enclose zircon, fluorite, allanite, iron oxides and zoned plagioclase (Fig. 7c). Feldspars are mostly masked by reddish brown hematitization (iron oxides staining). Some crystals are sericitized or kaolinitized due to alteration processes. Microcline perthites are rarely observed in this granite variety. Sometimes, Perthite crystals are surrounding by reaction rim (Fig. 7d).

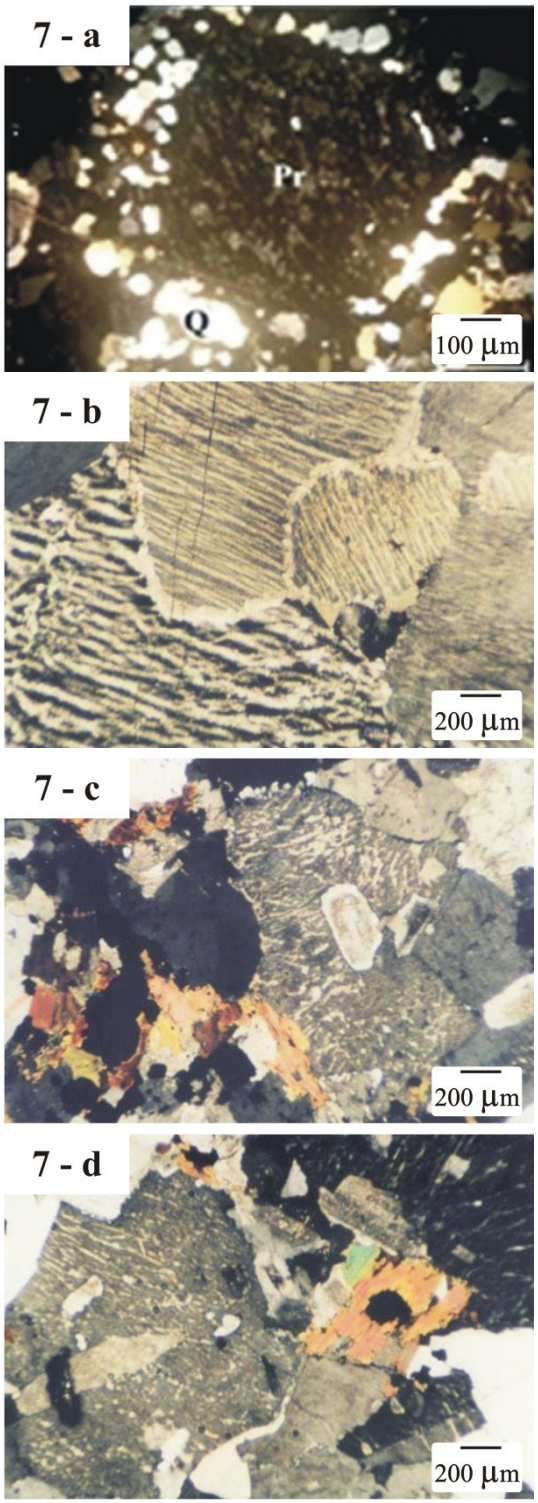

Fig. (7-a): Buck shoot of quartz (Q) on the boarder of perthite (Pr) in alkali feldspar granite, C.N.
Fig. (7-b): Subhedral crystal of perthite in alkali feldspar granite, C.N.
Fig. (7-c): Perthite crystal poikilitically enclose zoned plagioclase in alkali feldspar Granite, C.N.
Fig. (7-d): Perthite crystal surrounding by reaction rim in alkali feldspar granite, C.N.

Reaction rim attributed to the unmixing of the alkali feldspars which is preferentially located along the grain boundaries in the form of an albitic rim which nucleated and grew from the surface of the external grain (Pitcher 1993).

Quartz is less dominant than potash feldspars where it forms (40.9-45.5%) of the modal composition (Table 1). It occurs as colorless, anhedral crystals with various sizes. They generally occupy the interstitial spaces between the feldspar crystals. Some of them display wavy extinction and some have corrosive outlines against the string perthite crystals (Fig. 8a). Sometimes, quartz crystals show buck shoot shape on the boarder of perthite (Fig. 8b). In some parts of the rock, skeletal quartz crystals are enclosed in string perthite (Fig. 8c).

Plagioclase (An_{5-16}) occurs as anhedral to subhedral prismatic crystals ranging in sizes from 0.5 to 2.7 mm across and forms (1.5-2.91%) of the modal composition (Table 1). They show simple and lamellar twinning and corroded by quartz and perthites. Some crystals of plagioclase are partially altered to chlorite and saussurite especially along cores and fractures (Fig. 8d). Alteration starts from the core and propagates toward the peripheries reflecting higher contents of Ca within

the cores relative to the peripheries. Biotite flacks occur in minor amount mainly anhedral and strongly pleochroic from light brown to deep brown. They are partially or completely altered to chlorite (Fig. 8b). Some biotite flaks poikilitically enclose fluorite, iron oxides and zircon (Fig. 8a). Radioactive minerals are also associated with biotite.

Biotite flacks occur in minor amount mainly anhedral and strongly pleochroic from light brown to deep brown. They are partially or completely altered to chlorite especially along their peripheries (Fig. 8b). Biotite flacks are corroded by feldspars and quartz with different degrees until some islets are completely separated and surrounded by the other minerals. Some biotite flaks poikilitically enclose fluorite, iron oxides and zircon (Fig 8a). Radioactive minerals are also associated with biotite.

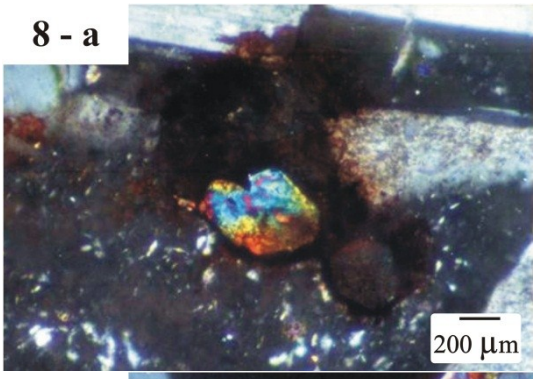

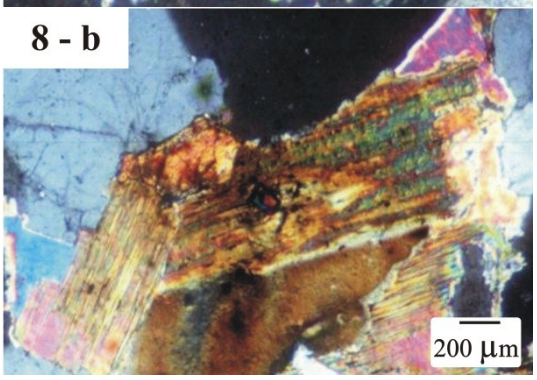

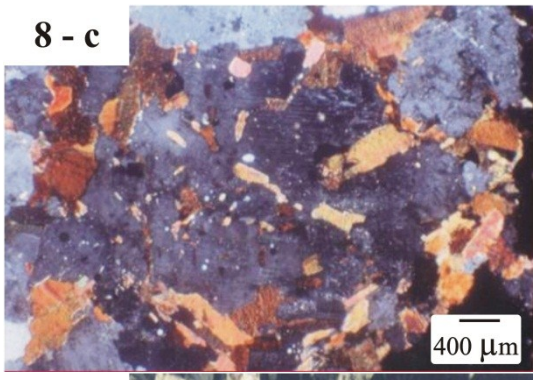

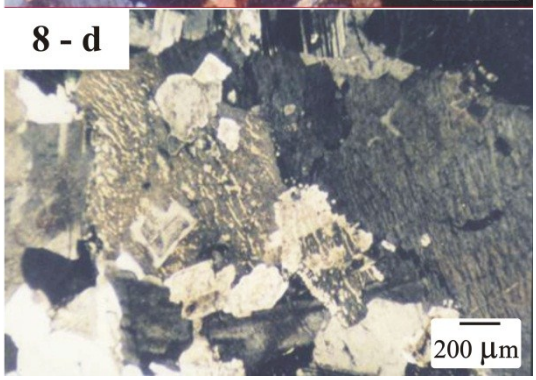

Fig. (8-a): Biotite poikilitically encloses zircon and iron oxide in alkali Feldspar Granite, C.N.
Fig. (8-b): Biotite flak altered to chlorite especially along its peripheries in Alkali Feldspar granite, C.N.
Fig. (8-c): Skeletal quartz crystals enclosed in string perthite in alkali feldspar Granite, C.N.
Fig. (8-d): Plagioclase crystal altered to saussurite especially along cores in Alkali Feldspar granite, C.N.

Muscovite occasionally associates biotite occurs as interstitial flakes between quartz and feldspars. It is found as colorless to pale yellow, small to medium irregular flakes and corroded by perthite and quartz (Fig. 9a). The occurrence of biotite and muscovite as hydrous minerals in these granites reflects their weak peraluminous nature (Barker, 1983). It also indicates a moderate abundance of water during the course of their crystallization. Fluorite is recorded as anhedral crystals. Apatite in

the form of minute prisms and needles are mostly recorded as inclusions in biotite, quartz and less commonly in feldspars. Opaques occur either as inclusions within biotite, quartz and feldspars (Fig. 9b).

Zircon is found as small subhedral to euhedral prismatic crystals. It is usually enclosed in quartz, feldspars and biotite (Fig. 8a, 9b). It is often associated with opaques, apatite, allanite and fluorite and rimmed with iron oxides. It is characterized by a very high relief and sometimes strong zoning. Some zircon crystals are occasionally metamicted and/or surrounded by strong pleochroic halos due to the radiogenic effects (Fig. 9b).

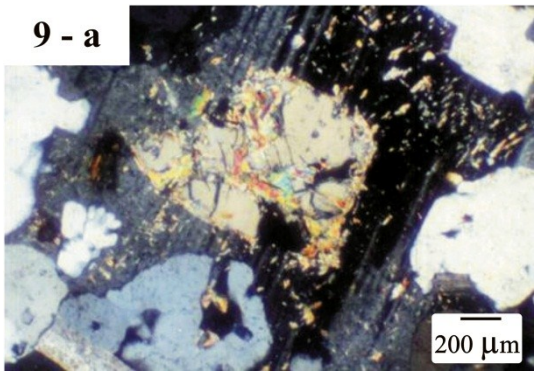

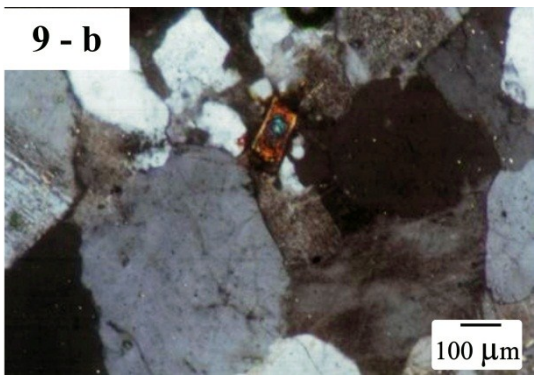

Fig. (9-a): Muscovite corroded by perthite and quartz in alkali feldspar Granite, C.N.

Fig. (9-b): Opaque crystal enclosed in perthite and Euhedral crystal of zoned zircon associated plagioclase in alkali feldspar granite, C.N.

4. GEOCHEMISTRY

The selected eight representative samples were subjected to chemical analyses. The chemical analysis for the major oxides (wt %) was done using wet chemical analysis technique of Shapiro and Brannock (1962) and El Reedy (1984) in the Analyses Department of the Nuclear Materials Authority of Egypt. The trace and rare earth elements (ppm) were measured by ICP-MS technique at the ACME analytical laboratories LTD, Vancouver, Canada. The obtained data with some geochemical ratios as well as the symbols used in the plotting for the studied granitic rocks are given in Table (2).

Rb/Sr ratio is a good guideline of typical magmatic differentiation where Rb tends to remain in the liquid phase while Sr tends to incorporate into plagioclase during fractional crystallization (Houghton, 1985 and Jelink et al., 1989). The ratio of Rb/Sr increases with magmatic differentiation due to Sr depletion in liquid magmas as a result of crystallization of feldspars, while Rb is higher in the liquid phase. In the present study, the alkali feldspar granites have a high and wide range of Rb/Sr ratios (from 16.69 to 30.13) suggesting that they are originated from highly differentiated magma.

The K/Ba ratio of the K_2O-Ba variation diagram that suggested by Mason (1966) and gave their crustal average ratio for granitic rocks as 65. In

the studied alkali feldspar granites the K/Ba ratios are higher than Mason's value (Fig. 10) reflecting depletion of Ba in source magma and /or advanced degree of magma differentiation (Hassan, 2001) and contribution of sialic crustal materials.

Table (2): The modal analysis Majors and traces of the studied younger granites

S. N.	1	2	3	4	5	6	7	8	9	10
SiO_2	74.95	74.75	75.5	74.53	74.74	74.47	74.21	73.82	73.93	73.73
TiO_2	0.03	0.03	0.02	0.02	0.01	0.02	0.03	0.04	0.06	0.04
Al_2O_3	12.63	13.33	12.58	12.05	12.63	12.92	13.11	13.31	12.96	13.46
Fe_2O_3	0.66	0.88	0.73	0.92	0.91	0.86	0.88	1.01	1.05	1.08
FeO	0.52	0.46	0.51	0.44	0.42	0.52	0.38	0.41	0.43	0.39
MnO	0.04	0.02	0.04	0.05	0.02	0.04	0.03	0.04	0.06	0.03
MgO	0.35	0.37	0.32	0.41	0.37	0.29	0.34	0.61	0.53	0.44
CaO	0.35	0.48	0.52	0.49	0.44	0.54	0.46	0.66	0.61	0.67
Na_2O	3.96	3.85	3.87	3.92	4.18	3.89	4.25	3.88	4.14	3.91
K_2O	4.51	4.81	5.14	5.39	5.02	4.71	4.77	4.39	4.57	4.44
P_2O_5	0.07	0.05	0.09	0.03	0.07	0.09	0.04	0.02	0.04	0.05
LOI	0.69	0.68	0.91	0.94	1.03	0.77	1.07	1.42	0.62	0.79
Total	**98.76**	**99.71**	**100.23**	**99.19**	**99.84**	**99.12**	**99.57**	**99.61**	**99**	**99.03**
Trace and rare earth elements (ppm)										
S. N.	**1**	**2**	**3**	**4**	**5**	**6**	**7**	**8**	**9**	**10**
Ba	85	71	69	82	77	63	58	88	79	86
Rb	241	263	267	244	257	255	239	291	265	280
Sr	8	14	16	13	9	11	14	12	9	12
Y	86	72	84	79	73	80	76	73	85	71
Zr	259	286	253	272	301	263	261	266	274	281
Nb	82	89	76	83	89	88	79	86	79	91
Pb	45	38	44	51	46	40	40	36	41	39
Ga	36	35	34	36	34	39	36	37	40	39
Zn	23	26	31	24	35	19	25	22	27	30
Cu	12	14	16	11	10	17	14	15	16	12
Ni	5	3	7	5	6	4	8	9	3	10
V	5	8	6	11	17	11	15	9	12	14
Cr	8	5	9	9	12	10	9	7	8	11
Co	4	3	6	5	7	4	5	3	6	3
Ca/Y	0.00	0.01	0.01	0.01	0.01	0.01	0.01	0.01	0.01	0.01
Ca/Sr	0.04	0.03	0.03	0.04	0.05	0.05	0.03	0.06	0.07	0.06
Rb/Sr	30.13	18.79	16.69	18.77	28.56	23.18	17.07	24.25	29.44	23.33
Ba/Rb	0.35	0.27	0.26	0.34	0.30	0.25	0.24	0.30	0.30	0.31
Zr/Sr	32.38	20.43	15.81	20.92	33.44	23.91	18.64	22.17	30.44	23.42
S.I.	10.65	11	11.25	11,67	11.53	10.98	11.28	10.69	11.19	10.82
K_2O/Na_2O	1.14	1.25	1.33	1.38	1.20	1.21	1.12	1.13	1.10	1.14

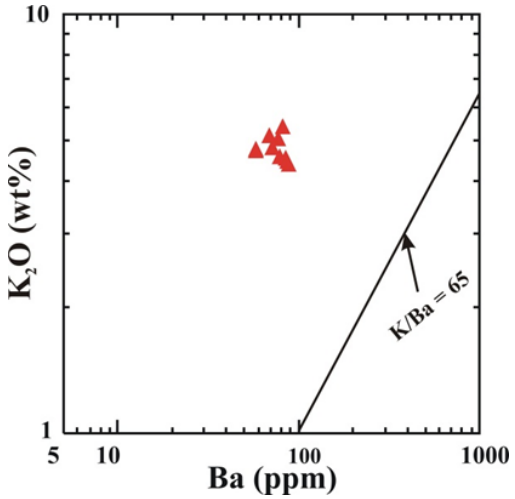

Fig. (10): K_2O (wt%) vs. Ba (ppm), (Mason, 1966)

Ca/Sr ratio values in the studied granitoids match the behavior of the two elements during the magma fractionation as suggested by Taylor and Heier (1965), where Sr tends to increase relative to Ca during the fractionation in these rocks hence Ca/Sr ratio values decrease during its magmatic crystallization.

The Ca/Y values decrease to reach its minimum as in the most differentiated granites (El-Gaby and Habib, 1982).

Cox et al., (1979) suggested that the K_2O/Na_2O ratio increases during the main stage of crystallization. The Na_2O/K_2O ratio of the studied granite ranges from 1.10 to 1.38 (Table 2), that indicates the granitoids origin of mantle.

Both granites are A-type granite characterized by calc-alkaline metaluminous with characteristic high K_2O/Na_2O.

Geochemical data revealed that the alkali feldspar granites were possibly originated from highly fractionated magma. This magma is rich in Rb and depleted in Ba and Sr. K/Ba ratio indicates an advanced magmatic differentiation. Also, the alkali feldspar granites display a rather limited standard deviation due to the narrow variation in their trace and major chemical constituents.

The ratio of Ba/Rb decreases with magmatic differentiation due to crystallization of feldspars. The average crustal ratio of Ba/Rb for granites, is as given by Chapman and Hall (1997).

In the present study, Ba/Rb ratio is ranging from 0.24 to 0.35 in, suggesting that the studied alkali feldspar granites were derived from a crustal material. The low ratio suggests that, they display a high degree of fractionation and relative enrichment in Rb in comparison to Ba in the source magma. This concept is supported by the strong negative correlation between Ba/Rb and Rb in the studied granitic rocks (Taylor, 1992 and Dostal and Chatterjee, 2000,).

Hall and Walsh (1969) suggested that the Zr/Sr ratio increase with increasing differentiation, indicating advanced degree of magmatic differentiation. They also added that the uraniferous granite is characterized by a high Zr/Sr ratio (more than 1.65). This concept is in complete harmony with the geochemical data of the studied granites (Zr/Sr ratio is more than 2).

The relation between SiO_2 and Major Oxides and trace elements revealed strong positive relation K_2O, Ba, Sr, and Y and normal with Na_2O, P_2O_5, Nb, Pb. while negative relation

with TiO_2, AL_2O_3, MgO, CaO and Fe_2O_3t. But it shows weak relations with Rb, Zr, Ga (Figs. 11, 12).

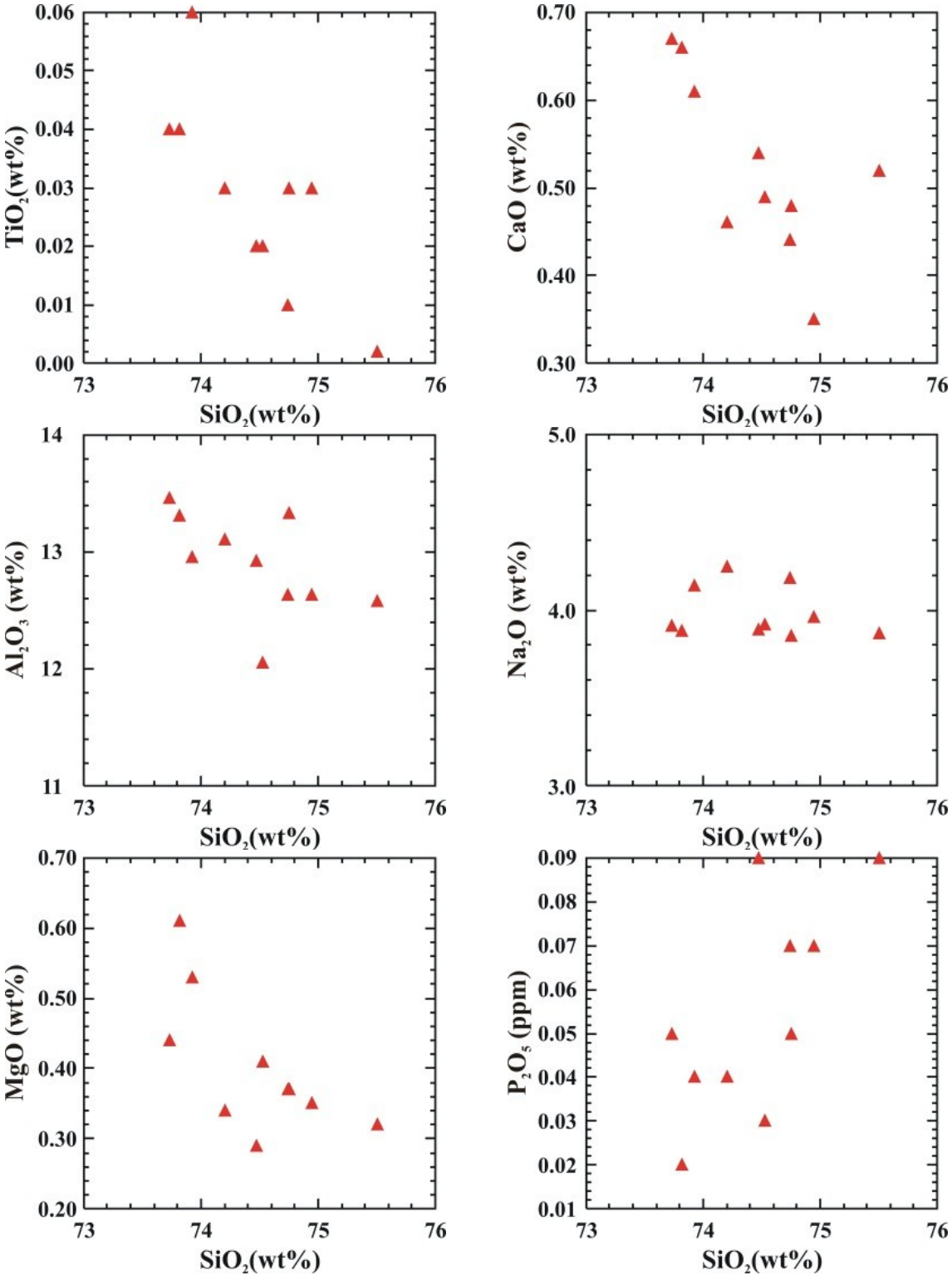

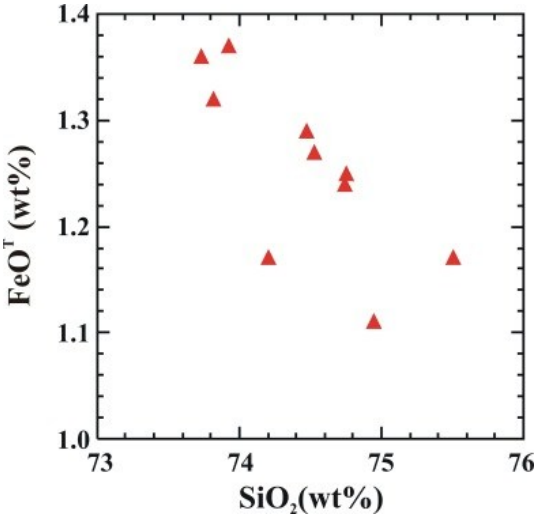

Fig. (11): Harker-type variation diagrams of some selected major vs. SiO_2 of the studied granitoids.

SOLIDIFICATION INDEX (S.I.).

Kuno (1959) stated that, the solidification index is equal to [(MgO/ ($MgO+Fe_2O_3+FeO+Na_2O+K_2O$)]×100. The analysed granitic samples have S.I values indicating that these granites formed from highly differentiated magma.

4.1. Geochemical classification and petrogenesis

Whalen et al. (1987) and Chapman (2005) took the Ga/Al ratio as a good guide for classification and types of magma where measuring the degree of differentiation in peraluminous and peralkaline granites. They suggested that the Ga/Al ratio increase from monzogranites (Ga/Al less than 0.0003) to syenogranites (0.0003<Ga/Al<0.0005) to alkali feldspars granite (0.0005<Ga/Al). This increase is due to an increase of Ga during the differentiation. In the studied alkali feldspar granitoids, the range of Ga/Al ratio values in Hamret Al-Jirijab is from 0.00051to 0.00056 classifying these rocks into alkali feldspar granites. This classification is in a complete harmony with their petrographic classification.

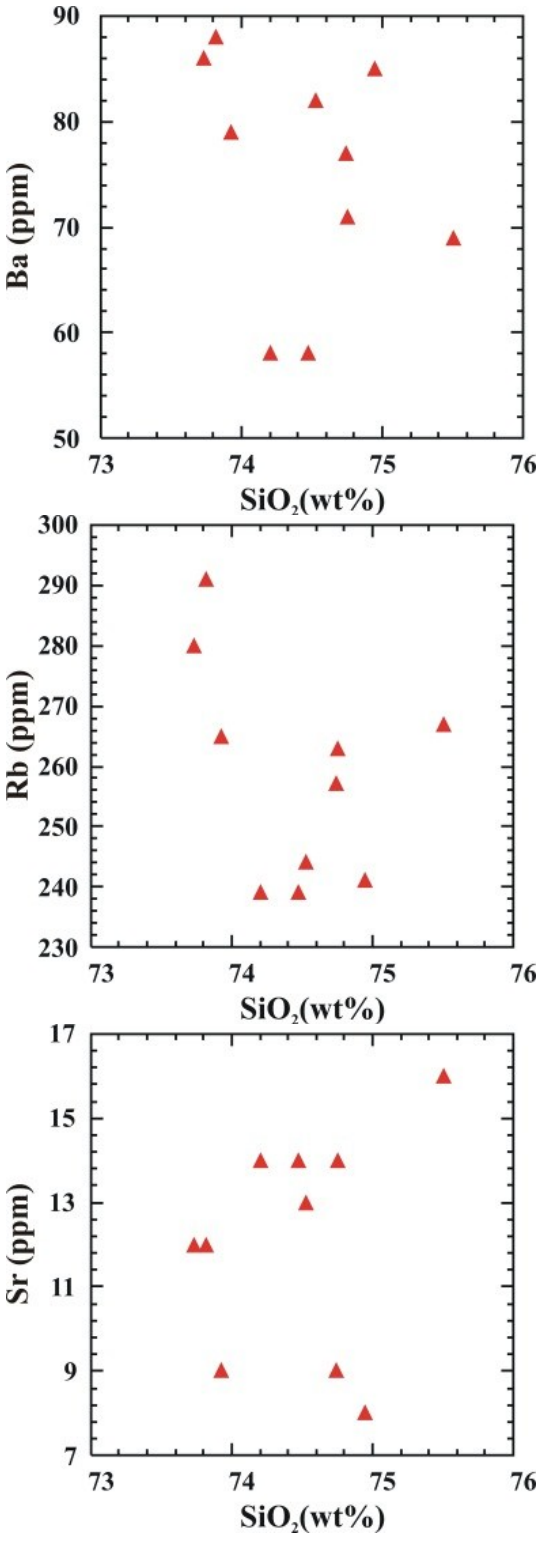

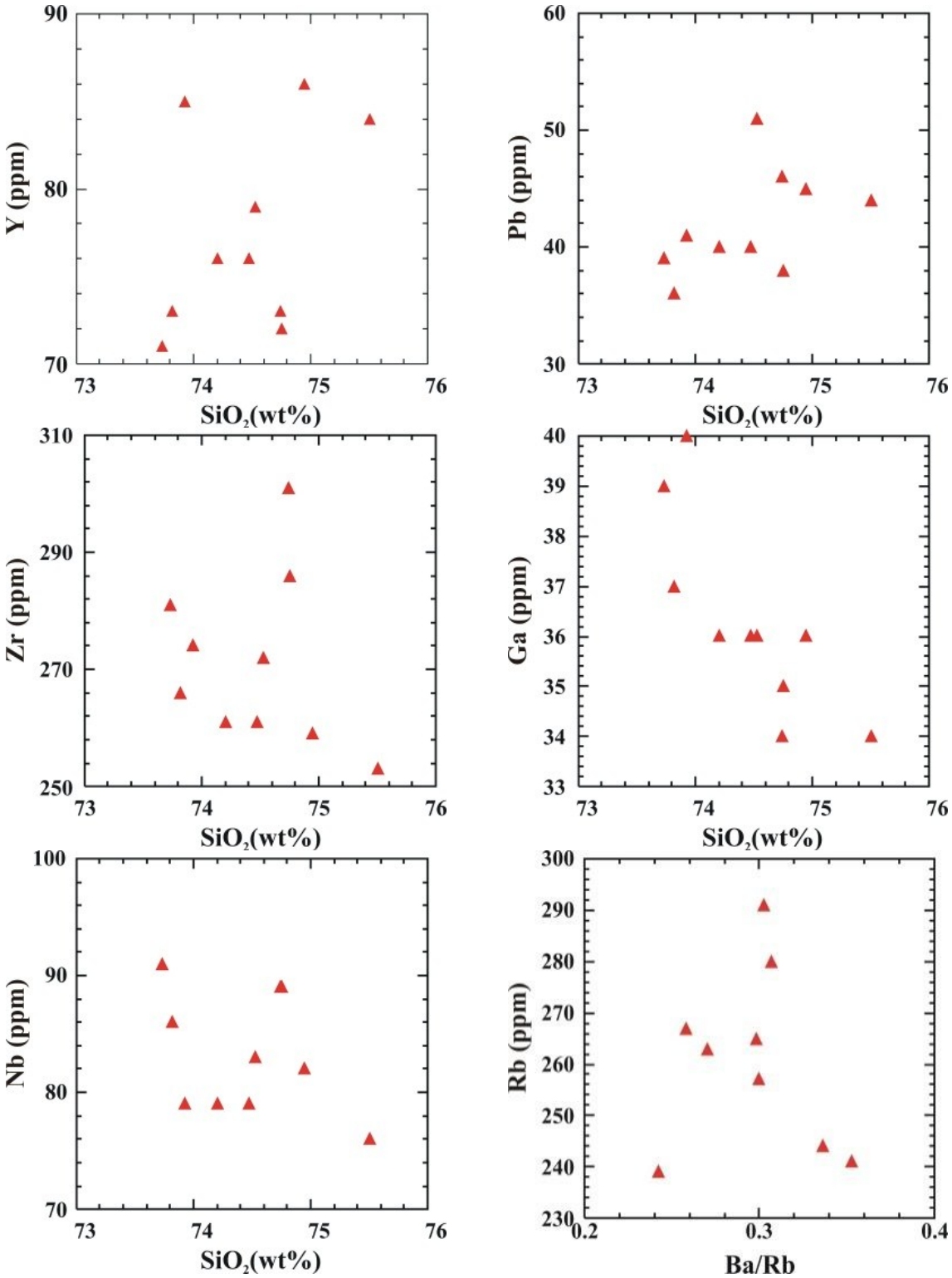

Figs. (12): Harker-type variation diagrams of some selected Trace elements (ppm) vs. SiO_2 of the Studied granitoids

The studied granitoids have been classified in the chapter of petrography

using their modal composition on the Streckeisen (1976) diagram as alkali-feldspar granites.

On the binary diagram of SiO_2 and (Na_2O+K_2O) of Middlemost, (1985) and Middlemost (1994), the majority of the granitic samples plot mainly in the granite and some of them are very close to its boundary with the alkali-feldspar granite fields. O'Connor (1965), also used the Ab-Or-An ternary diagram as shown in (Fig. 13) all the granites plot in the granite field.

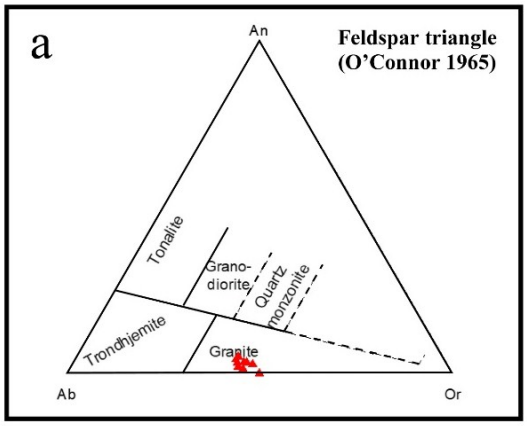

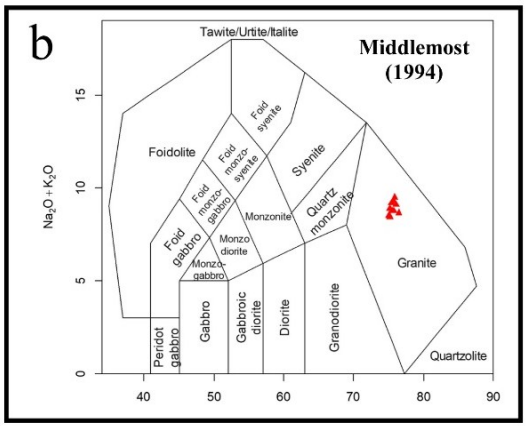

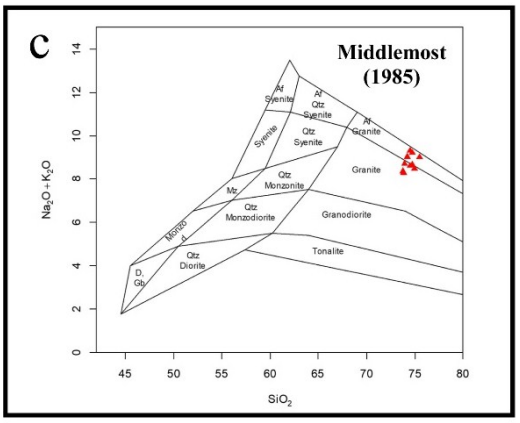

Fig (13) a): Normative Ab-An-Or diagram, (O'Connor, 1965), b and c) SiO_2-(Na_2O+K_2O) binary diagrams, (Middlemost, 1985 and 1994)

4.2. Types of granite

Whalen et al. (1987) used Mol. 10000*Ga/Al with (Na_2O+K_2O/CaO), (Na_2O+K_2O), Zr, Nb, K_2O/MgO, FeOt/MgO, Y and Zn to differentiate between types of Granites; using these relations (Fig. 14), all the studied granitoids rocks plot in the A-type field indicating igneous precursors of the studied granitic rocks.

Granitoids rocks are described using Shand's index as: peraluminous (A/CNK >1), metaluminous (A/NK >1 and A/CNK <1) and peralkaline (A/NK < 1) using molar ratios (A = Al_2O_3, C = CaO, N = Na_2O and K = K_2O). On the studied granites, the A/CNK ratio is more than 1 suggesting the peraluminous affinity for the studied granitoids. Villaseca et al., (1998) and Ragab and El-Gharbawi (1989) suggested that most of peraluminous Egyptian younger granites have been formed from crustal materials (Fig. 15).

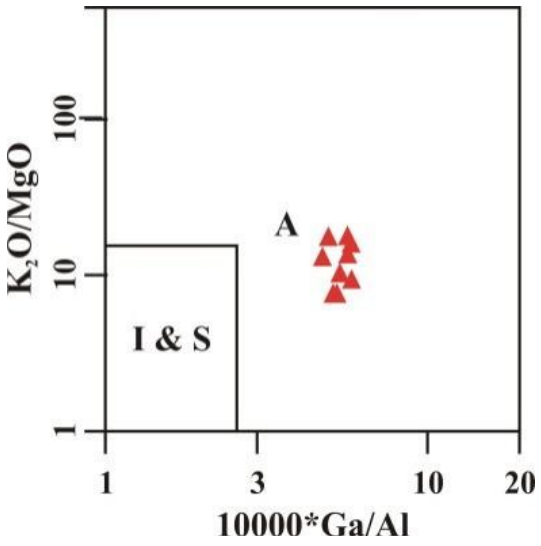
K2O/MgO
100
10
1
A
I & S
1
3
10
20
10000*Ga/Al

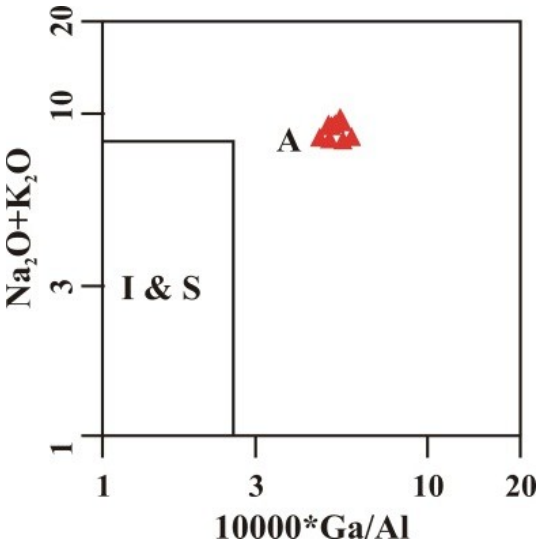
Na2O+K2O
20
10
3
1
A
I & S
1
3
10
20
10000*Ga/Al

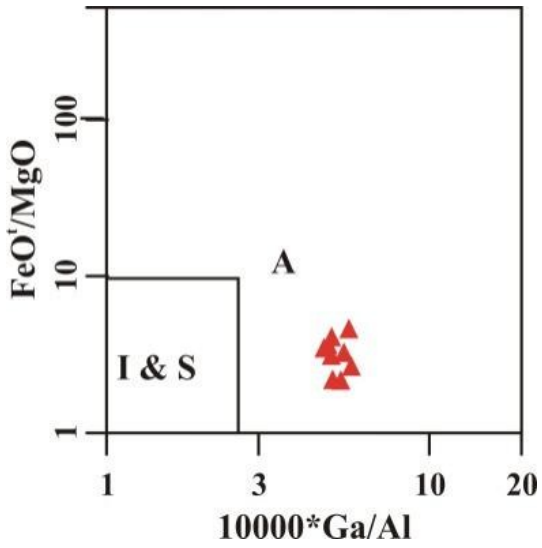
FeO'/MgO
100
10
1
A
I & S
1
3
10
20
10000*Ga/Al

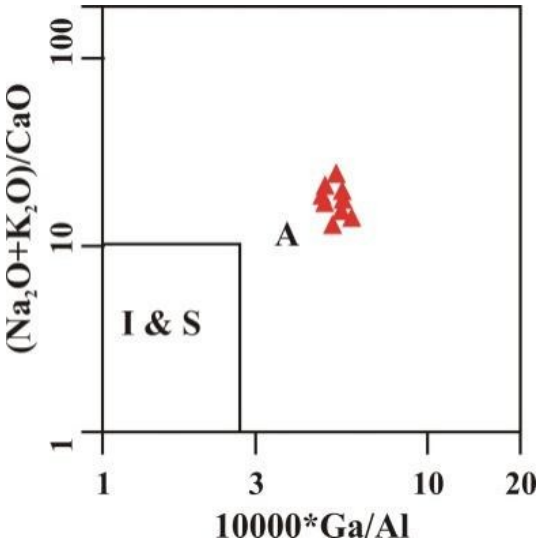
(Na2O+K2O)/CaO
100
10
1
A
I & S
1
3
10
20
10000*Ga/Al

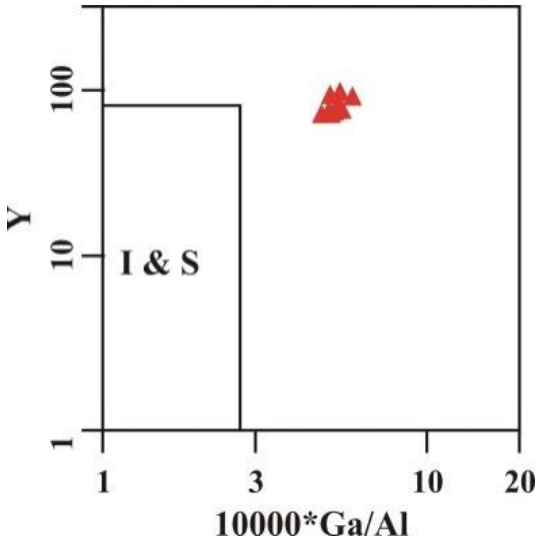
Y
100
10
1
I & S
1
3
10
20
10000*Ga/Al

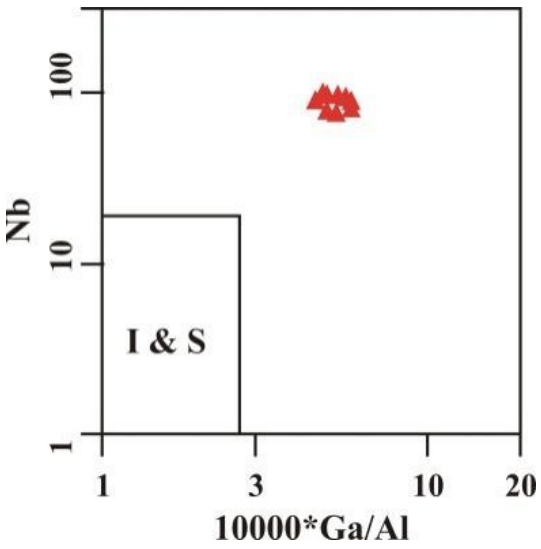
Nb
100
10
1
I & S
1
3
10
20
10000*Ga/Al

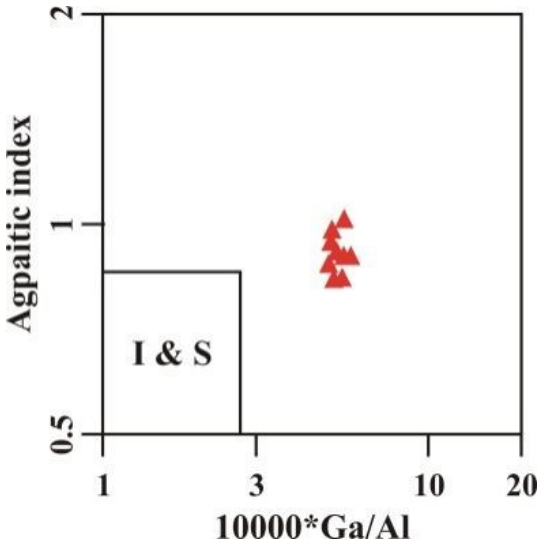

Fig (14): Whalen et al., (1987) discrimination diagrams (10000Ga/Al) ratio against Na_2O+K_2O, Na_2O+K_2O/CaO; K_2O/MgO; FeO^t/MgO, Zr, Nb, Zn and Y

4.3. Magma type and tectonic setting

Maniar and Piccoli (1989) variation diagrams used to discriminate between the different tectonic settings. (Fig. 16) shows that the studied granitic samples are mainly plot in the POG field. This interpretation could be supported by the field relationships and observations because the younger granites intrude all the pre-existing rock types exposed in the area and also they do not show any sign of large scale metamorphism or even foliation. The studied granites plot between 1 and 2 kb water vapor pressure. Their plots lie near or at the center of the diagram suggesting that the crystallization occurred at temperatures ranging from 800 ^oC to 850 ^oC.

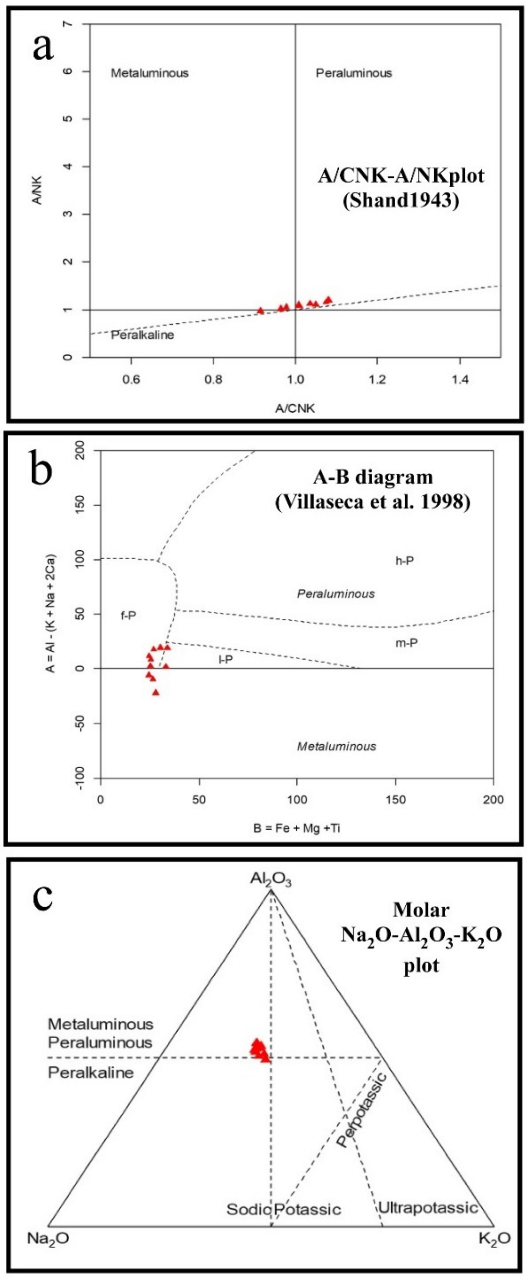

Fig (15): a) Alumina-saturation Shand, (1943), b) Villaseca et al (1998) and c) Na_2O-K_2O-Al_2O_3 diagram (Bonin, 1972)

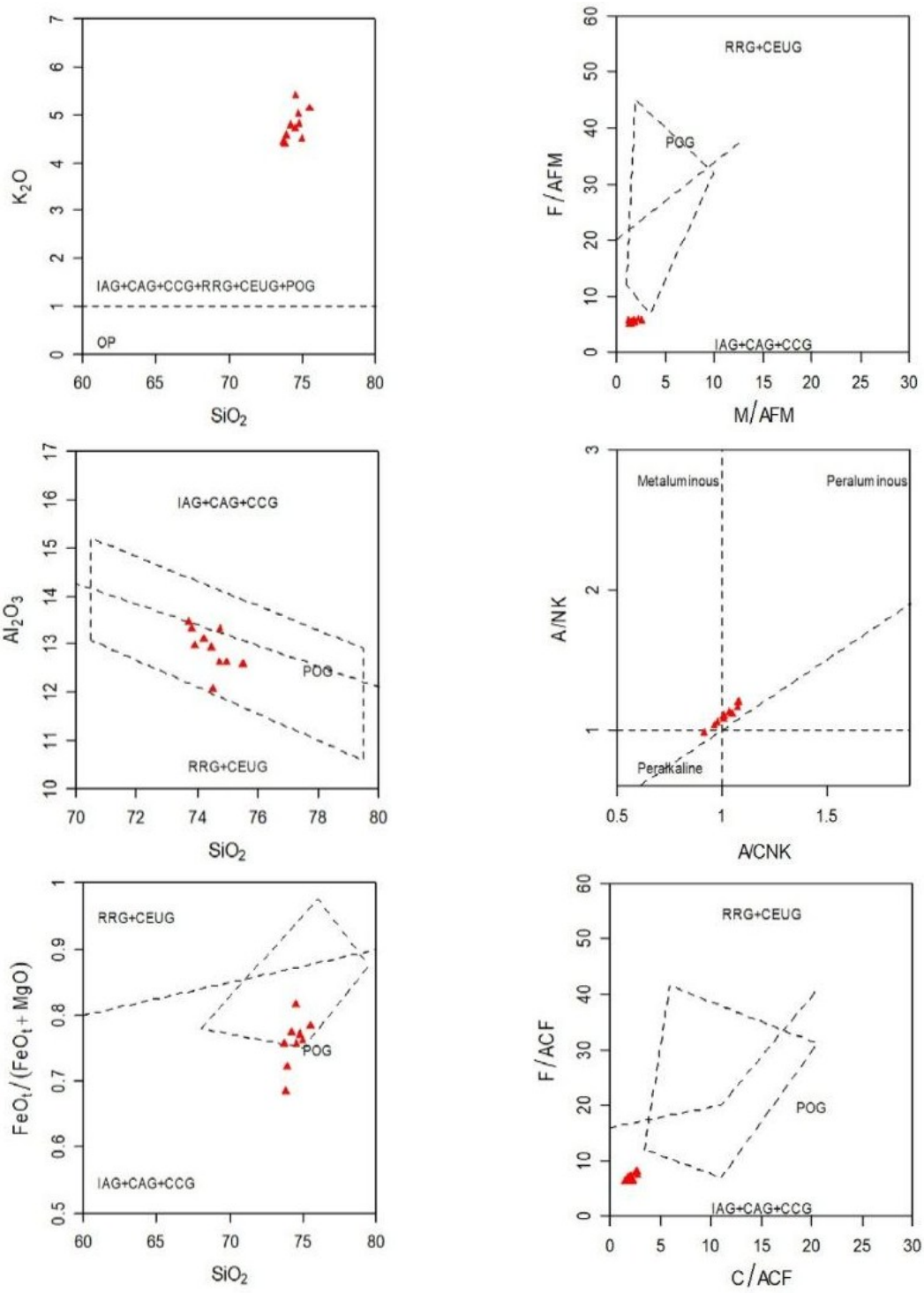

Fig (16) Tectonic setting diagrams Maniar and Piccoli (1989) for the studied granitoids.

4.4. Geochemistry of Rare Earth Elements (REES)

REEs are a useful geochemical tool to supply valuable information about rock genesis. From the REEs data (Table 3) and chondrite normalized pattern (Fig. 17), important inferences can be summarized as follow:

1- The REE chondrite pattern of the studied alkali feldspar granite shows decisive irregularities (often referred to as tetrads or lanthanide tetrad effect which is shown by two concave – upward segments (t1: La to Nd and t3: Gd to Ho), (Henderson, 1996).

2- This tetrad effect with the non-CHARAC behavior of Zr and Hf and the low Zr/Hf ratio are indications of highly evolved granites (e.g. Bau, 1996 and Irber, 1999).

3- The chondrite normalized pattern of the alkali feldspar granites is distinguished by strong negative Eu anomaly and high $SLREE/SHREE_N$. The marked deficiency of Eu in the studied alkali feldspar granites is an immediate expression of increasing alkalinity. The development of negative Eu anomaly with increasing in K content must be due to the progressive separation of plagioclase at low pressure and crystallization of K-feldspars. The higher $(SLREE/SHREE)_N$ ratio with increasing in Si and K and incompatible elements content is another evidence that the alkali feldspar granites are of more differentiated stage (Fig. 17).

Table (3): The modal analysis REE, U and Th of the studied younger granites (ppm)

S. N.	1	2	3	4	5	6	7	8	9	10
U	12.1	16.1	11.4	15.3	16.7	12.2	14.5	13.1	16.3	14.2
Th	26.2	29.4	23.5	28.5	29.4	27.5	28.1	27.5	30.2	28.4
La	51,1	49.8	50.3	53.6	54.5	55.3	53.6	55,3	56.1	55.2
Ce	120.7	121.9	125.2	120.4	122.5	130.1	126.3	121.7	123.5	122.3
Pr	27.5	26.9	31.2	30.8	28.6	31.1	29.8	28.7	30.1	27.9
Nd	29.8	31.7	34.7	33.5	35.3	32.6	34.7	34.6	33.1	32.8
Sm	8.5	9.7	8.7	8.9	9.4	9.1	8.7	7.9	8.4	9.6
Eu	0.4	0.3	0.3	0.4	0.3	0.5	0.3	0.4	0.3	0.3
Gd	7.5	8.1	7.8	7.7	8.3	6.9	7.4	8.1	7.7	8.6
Tb	1.5	1.3	1.4	1.4	1.6	1.4	1.2	1.5	1.3	1.4
Dy	25.4	26.3	26.7	24.1	26.4	24.3	25.1	24.2	26.6	23.9
Er	2.2	1.8	1.6	2.0	2.1	1.8	1.9	1.7	1.8	1.9
Yb	8.5	8.8	9.1	8.6	9.3	9.1	9.4	8.7	9.8	8.2
Lu	0.6	0.5	0.6	0.6	0.4	0.6	0.4	0.3	0.4	0.5
Geochemical ratios										
S. No	1	2	3	4	5	6	7	8	9	10
Eu*	0.28	0.11	0.28	0.27	0.13	0.12	0.25	0.14	0.28	0.11
L/H	6.30	6.20	6.27	6.77	6.66	6.90	6.92	7.00	6.30	6.20
Ce/Nb	1.47	1.51	1.49	1.47	1.53	1.47	1.53	1.44	1.47	1.51
Yb/Ta	2.83	2.93	3.00	2.87	2.37	3.07	2.77	2.67	2.83	2.93

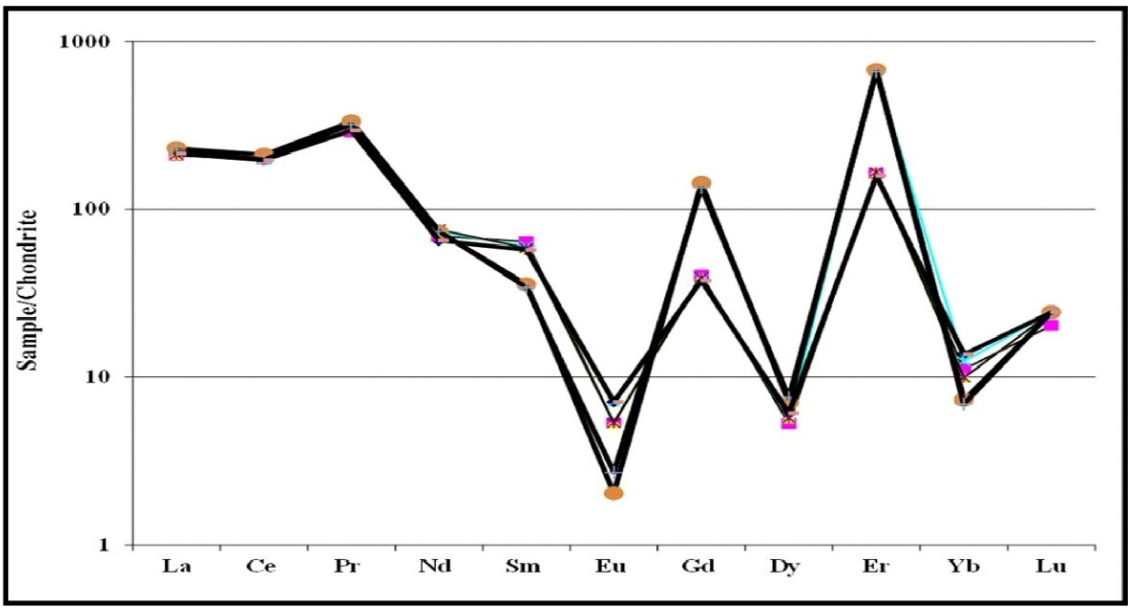

Fig. (17): The average concentrations of the chondrite - normalized rare earth elements patterns of the studied alkali feldspar granites of Hamret Al-Jirjab, Esh El Mellaha area

5. RADIOACTIVITY

The measurements of gamma rays spectrometry will express the eU, eTh, Ra in (ppm) and K in (%) rather than the actual concentrations of uranium and thorium themselves as the uranium and thorium are not gamma-emitters but their radiation is related to their daughters.

The natural radioactivity of rocks mainly stems from their contents of U, Th and K^{40}. Generally, during magmatic differentiation, U and Th increase from basaltic to low Ca-granitic rocks, but the Th/U ratio remains constant. Cambon (1994) stated that, the U content of the different rock types is variable. The types, which contain most of the U, are the post-orogenic granitic rocks. Generally, in granitoid rocks, the uranium content is mainly controlled by the amount and type of accessory minerals (Darnley, 1982; Moharem, 2002 and Gouda, 2007).

The eU, eTh, Ra in (ppm) and K in (%) are shown in Table (4) for the studied samples. The average contents of eU and eTh in the studied rocks and different rock types given by several authors are given for comparison.

Seven samples were collected from Hamrat Al-Jirjab alkali feldspar granites and radiometrically analysed. They show U content ranges between 13 and 21 ppm with an average of 16.86 ppm. The Th content ranges from 28 to 39 ppm with an average of 34.14 ppm. The Th/U ratio ranges from 1.48 to 2.85 with an average of 2.08. Radium content (Ra) ranges from 8 to 14 ppm with an average of 10.43 and. Potassium content (K) ranges from 3.32 to 3.79 with an average 3.49%. (Table 4).

Accordingly, the alkali feldspar granites of Hamrat Al-Jirjab have relatively higher average U and Th content than the other types of granites given by the previous authors. indicates

that the alkali feldspar granites of Hamrat Al-Jirjab have lower Th/U ratios than the world averages. This means that the studied alkali feldspar granites in the studied area are higher in uranium relative to thorium.

Table (4): Results of radiometric analyses of some samples collected from the Alkali feldspar granite of Hamrat Al-Jirjab area

S. N.	eU (ppm)	eTh (ppm)	Ra (ppm)	K (%)	eU/Ra	eU/eTh	eTh/eU
1	15	38	9	3.32	1.7	0.39	2.53
2	13	37	9	3.60	1.4	0.35	2.85
3	21	31	14	3.29	1.5	0.68	1.48
4	20	39	11	3.62	1.8	0.51	1.95
5	16	28	8	3.79	2.0	0.57	1.75
6	18	34	12	3.37	1.5	0.53	1.89
7	15	32	10	3.43	1.5	0.47	2.13
Av	16.86	34.14	10.43	3.49	1.63	0.50	2.08

Moreover, Darnley (1982) defined the nearly uraniferous granites as any granitic mass containing U at least twice the Clark value (4 ppm) for normal granites (Clark et al., 1966). This means that any granite containing 8 ppm U and/or 40 ppm Th is named as nearly uraniferous granite. Such granite may or may not be associated with U-mineralization. These values of eU and eTh in the studied granite are attributed to the presence of U and Th bearing accessory minerals as zircon, allanite and fluorite.

5.1. Radio-elements relationships

U, Th, REEs, Zr and Nb behave incompatibly in a granitic melt so that, where U concentration is controlled by magmatic processes, these elements would be expected to increase (Cuney, 1984). The relation between U and Th may indicate the enrichment or depletion of U because Th is chemically stable. Normally, thorium is three times as abundant as uranium in all rock types (Darnley, 1982). When this ratio is disturbed, it indicates either depletion or enrichment of uranium. These relationships indicate that uranium enrichment was mainly controlled by primary magmatic processes.

6. RADIOACTIVITY MEASUREMENTS

6.1. Gamma spectrometer

6.1.1. Samples preparation

Seven samples were collected from Hamrat Al-Jirjab alkali feldspar granites and radiometrically analysed, the samples crushed mechanically into a powder form, then dried and ground to have a 100 mish size. These homogenized samples each are weighting 200 g each one was packed into a polyethylene circular containers (Merinelli beakers) of 10 cm diameter and 3 cm height. each sample was pressed manually in its container until it was filled and then it is closed tightly and stored, at least it was sealed for about one month to be reach the state of sequiller equilibrium between radium (^{226}Ra) and its decay product that are comprise 98.5% of the radiological impact of the uranium series. The

contributions of uranium and its decay products of radium are ignored. Therefore, the reference of uranium series radionuclides is usually written as radium instead of uranium, (Farai et al, 2005). A multi-channel analyzer of gamma- ray spectrometry Na I (Tl) detector that have high efficiency that was used for measuring the concentration of uranium, thorium, radium and potassium. These analyses has been carried out in the laboratory of chemical prospection at Egyptian Nuclear Materials Authority. Measurements are obtained in ppm and then converted to (Bq/kg), the specific activity concentrations (Bq/kg) of each sample was computed, **(IAEA-2003)**.

6.1.2. Gamma absorbed dose rate in air (DR)

The absorbed dose rate had been calculated according to the gamma radiation in the air at 1 m above the ground surface. The conversion factors used for DR calculations are 0.462 nGy/h for ^{226}Ra, 0.621 nGy/h for ^{232}Th, and 0.0417 nGy/h for ^{40}K. (DR) can be calculated as follow. (UNSCEAR, 2008).

DR = 0.462 ARa + 0.604 ATh + 0.0417AK (1)

In order to evaluate radiological risk, external exposure to radiation arising from NORM is determined in terms of the absorbed dose rate in air at 1 m above the ground surface since; AU; ATh and AK are the activities of ^{238}U, ^{232}Th and ^{40}K, respectively, in Bq/kg.

6.1.3. Annual effective dose (AED).

The annual effective dose rate in (mSv/y) can be calculated using the following equation (Abdel-Razek et al., 2016): AED = DR × 8760 × 0.7 × 0.2 × 10− 6 (2)

Where 0.7 Sv/Gy is the conversion coefficient from the absorbed dose to the effective dose, and 0.2 is the fraction of time spent outdoors.

6.1.4. Excess lifetime Cancer risk (ELCR)

The ELCR gives the probability of cancer developing over a lifetime at a given exposure level. The ELCR is calculated using the following equation, (Abbasi et al 2018):

ELCR= AED (mSv/y) * (DL) * (RF) * 10-3 (3)

Where DL is the average life span (70 years) and RF is the coefficient risk factor per Sv. the ICRP uses RF as 0.05 for the general public. The world average of 0.3 also taken as the recommended limit (ICRP, 2007).

6.1.5. Annual Gonadal equivalent dose (AGED)

The annual gonadal equivalent dose (AGED) according to the specific activities of Ra-226, Th-232 and K-40 was computed using the following equation, (Arafa, 2004).

6.1.6. AGED (μSv/y) = 3.09 ARa + 4.18 ATh + 0.314 AK < 300000 (4)

The standard guideline for AGDE set by (UNSCEAR. 2000) is 300000 (uSv/y).

6.2. Results and discussion

The mean activity concentrations of ^{238}U, ^{226}Ra, ^{232}Th and ^{40}K were found

to be 208.19, 115.76, 138.62, and 1091.92 Bq/kg with ranges from 160.55 to 259.35 Bq/kg, 88.8 to155.4 Bq/kg, 113.68 to 158.34 and 1029 to 1186.27 Bq/kg, respectively, (table 5). Overall The presently obtained values, were greater than the worldwide average 33, 32, 45, and 412 Bq/kg for uranium, radium, thorium, and potassium, (UNSCEAR, 2008).

The highest values of the absorbed dose rate, DR was 257 nGy/h, with a mean value of 225.44 nGy/h, table (5). These values of DR was higher than the worldwide average values of 58 nGy/h for public, (UNSCEAR, 2008).

The mean values of annual effective dose of public AED were 0.28 mSv/y, and they ranged from 0.26 to 0.32, (mSv/y), table (5). The annual effective dose of public that was almost within the limits according to the world wide average for public 1(mSv/y), (UNSCEAR, 2008).

The excess life cancer risk, values had been assessed in this study depend on (AED). The value of ELCR were ranged between 0.9* 10-3 to 1.1* 10-3 respectively with the mean value 0.97, table (5). The excee life cancer risk value are higher than the world wide range 0.29*10-3, (UNSCEAR, 2008).

The annual gonadal dose equivalent, data range alternated between 1122.06 to 1394 (uSv/y), with the mean value of 1279.98 uSv/y table (5). Which lower than the approved limit of 300000 (uSv/y), (UNSCEAR, 2008).

Table (5): Activity concentrations of ^{238}U, ^{226}Ra, ^{232}Th,and ^{40}K (Bq/kg), Absorbed dose rat (DR), annual effective dose (AED) Excess lifetime cancer (ELCR), Annual gonadal dose equivalent (AGDE) due to Granite samples

S. N.	^{238}U	^{226}Ra	^{232}Th	^{40}K	D_R	AED	ELCR	AGDE
1	185.25	99.9	154.3	1039.2	222.10	0.272	0.95	1279.9
2	160.55	99.9	150.2	1126.8	211.89	0.260	0.91	1290.4
3	259.35	155.4	125.9	1029.8	238.78	0.293	1.02	1329.6
4	247.00	122.1	158.3	1133.1	257.00	0.315	1.10	1394.9
5	197.60	88.8	113.7	1186.3	209.42	0.257	0.90	1122.1
6	222.30	133.2	138.0	1054.8	230.06	0.282	0.99	1319.8
7	185.25	111.0	129.9	1073.6	208.83	0.256	0.90	1223.2
average	208.19	115.76	138.62	1091.92	225.44	0.28	0.97	1279.98
worldwide	33	32	45	412	58	1	0.29	300000

7. CONCLUSIONS

Esh El Mellaha area represents a part of the north western extension of the Arabo-Nubian shield. It forms an elongated ridge parallel to the Gulf of Suez, running in NW-SE direction. In Esh El Mellaha range, the younger granites crop-out in the form of three intrusions. These younger granites are mostly represented by Gabal Um Dirra monzogranites, Gabal El-Esh syenogranites and Gabal Hamret Al-Jirjab alkali feldspar granites.

The alkali feldspar granites (G. Hamret Al-Jirjab) are medium- to coarse-grained, hypidiomorphic rocks, and are essentially composed of perthites, quartz, plagioclase, muscovite and biotite. The accessory and secondary minerals are zircon, sphene, apatite, epidote, fluorite and iron oxy-hydroxides. The alkali feldspar granites show high perthites (reach up 58%), the increase in perthites is accompanied by increase in quartz and decrease in the plagioclase contents. They show high contents of deep violet fluorite and metamicted zircon as well as high contents of iron oxides.

Geochemically, these granites were originated from peraluminous calc-alkaline highly fractionated magma. This magma is also rich in Rb and depleted in Ba indicating low pressure condition. The granites are alkali feldspar classified and A-type were originated from peraluminous and POG setting. They originate in post-orogenic environment and could be considered as mesozonal granites. The REEs chondrite patterns are indication of the common source, although the alkali feldspar granites are relatively more differentiated.

The REEs chondrite normalized patterns and geochemical ratios suggest that the studied alkali feldspar granites are differentiated from monzogranites or at least originated from similar magma and tectonic setting.

The remaining zigzag effect of the chondrite-normalized patterns can be interpreted to possible “tetrad-effect”. The development of lanthanide tetrad effect and the non-CHARAC behavior of Zr and Hf indicate that the studied alkali feldspar granites are a partial melt extracted from monzogranites.

Although the average U contents (X`) is higher than normal granites and the geochemical markers (e.g. felsic index, Rb/Sr, Th, Nb, Rb and Zr) of the studied granites match well with those of the uraniferous granites. The studied granites cannot be considered as fertile granites according to the statistical parameters (S and C.V.). The low S and C.V. values means that the uranium content of these rocks is syngeneic and are not favorable for mineralization, because of missing late remobilization. This assumption is also witnessed by the strong correlation between Th and U.

Accordingly, the studied younger granites are considered as uraniferous granites originated from a fractionated U-rich magma with trapping high concentrations of uranium in accessory minerals. The alkali feldspar granites show high U and Th contents and low Th/U ratios due to the higher quotient of the radioactive accessory minerals (e.g. zircon, apatite and allanite) with addition of fluorite. The measurement of activity concentrations of U-238, Ra-226, Th-232, and K-40 achieved to assess the radiological health hazards for public, in the studying samples, such as absorbed dose rate, annual effective dose rate, excess lifetime cancer and annual gonadal equivalent dose that may cause risk for individuals living in around the study area. The mean activity

concentrations values of ^{238}U, ^{226}Ra, ^{232}Th, and ^{40}K, in the studying samples were higher than the worldwide limit. The absorbed dose rate values in air were exceeded the world wide average, the estimated values of both annual effective dose and annual gonadal equivalent dose in the studying samples were accepted with the recommended limit. The ICRP-60 has recommended that any exposure higher than the natural radiation background should be kept as ALARA principal but below the individual dose limits, which for members of the public is 1 mSv/y. The ELCR is an additional risk that public that may be getting cancer if they have been exposed to cancer-causing materials for a longer time. The excess lifetime cancer risk estimated values are also higher than the world average limit $0.29*10^{-3}$. These results indicate that the public that was received higher effective doses due to high radioactivity, and they must take all precautions and protection against the high radioactivity. This reflects the U-minerals bearing in the studied area and this area can be classified as a high background radiation area, and proper precautions need to be taken.

Acknowledgements The authors sincerely would like to thank the anonymous reviewers for their comments that help improve this manuscript significantly. Special thanks to the reviewers for their encouraging comments and annotations that greatly improved an earlier version of the manuscript.

REFERENCES

Abbasi, A., Mirekhtiary, F., Mirekhtiary, S.F., 2018. Risk assessment due to various terrestrial radionuclides concentrations scenarios. Int J Radiat Biol.

Abd El Baset, 2013. mineralogical and geochemical prospection and radioelements distribution in Hamrat Al-Jirjab stream sediments, Esh el Mellaha range north eastern desert Egypt Ph. D. Thesis, Cairo University. 225p.

Abdel-Razek, Y. A., Masoud, M. S., Hanfi, M. Y., El-Nagdy, and M. S., 2016. ScienceDirect radiation doses from natural sources at seila area south eastern desert, Egypt. Journal of Taibah University for Science 10, 271–280.

Arafa, W., 2004. Specific Activity and Hazards of Granite Samples Collected from the Eastern Desert of Egypt. Journal of Environmental Radioactivity, 75, 315-327. https://doi.org/10.1016/j.jenvrad.2004.01.004

Barker, D.S., 1983. Igneous rocks. Prentice, Hall. Inc. Englewood Cliffs, USA, 287 pp.

Bau, M., 1996. Controls on the fractionation of isovalent trace elements in magmatic and aqueous systems; evidence from Y/Ho, Zr/Hf, and lanthanide tetrad effect. Contribute Mineral Petrol V. 123, p. 323-333.

Bentor, Y.K., 1985. The crustal evolution of the Arabo-Nubian Massif with Special reference to the Sinai

Peninsula. Precam. Res., V. 28, P. 1-74.

Bonin, B., 1972. Les complexes granitiques subvolcaniques de la region de Tolla-Cauro (Corse), these 3 semc cycles, Paris VI. Published in Labo, Geol., E N S, and No. 7,127p.

Cambon, A. R., 1994. Uranium deposits in granitic rocks. Notes on the national training course on uranium geology and exploration. Organized by IAEA and NMA, 8 - 20 Jan. 1994.

Chapman, C.A., 2005. Petrogenesis of granitic rocks. Boundary Row, London. 225p.

Chapman, C.A., and Hall, A., 1997. The nature and origin of granite. Boundary Row, London. 387p.

Clark, S.P.Jr.; Petrman, Z.E. and Heier, K.S., 1966. Abundance of uranium, thorium and potassium, In: S.P. Clark, Jr., (Editor), Handbook of Physical constants, Geological Society of American Bulletin V. 97, Section 24, p. 521 - 541.

Cox, K.C., Bell, J.D., and Pankhurst, R.J., 1979. The interpretation of igneous rocks. William Clowes, London, Britain, 414p.

Cuney, M., 1984. Les methods des prospection de l'uranium, Nuclear Energy Agency of the OECD, Paris. p. 277-292.

Darnley, A.G., 1982. "Hot granites" Some general remarks, In: Maurice, Y. J. (ed.), and Uranium in granites. Geol. Surv. Canada, paper No. 81-23, p. 1-10.

Dostal, J., and Chatterjee, A.K., 2000. Contrasting behaviour of Nb/Ta and Zr/Hf ratios in a peraluminous granitic pluton, Nova Scotia, Canada. Chem. Geo. V. 163, p. 207-218.

El Gaby, S., and Habib, M.S., 1982. Geology of the area southwest of Port Safaga with special emphasis on the granitic rocks. Eastern Desert, Egypt. Ann. Geol. Surv. Egypt, Vol. 12, p. 47-71.

El Reedy, M.W., 1984. The general, physical and chemical features and the pollution level of El Sabahia-Sabhan-El Requa soil localities, State of Kuwait. Report represented to environmental protection Dept. Ministry of Public Health, Kuwait (Part I: chemical methods).

Farai, I.P., Ademola, J.A., 2005. Radium equivalent activity concentrations in concrete building blocks in eight ies in Southwestern Nigeria. J Environ Radioact 79:119–125.

Gouda, M.A., 2007. Geological and geochemical studies on some younger granitic rocks, north Eastern Desert, Egypt. Ph. D. Thesis, Al-Azhar University. 261p.

Hall, A., and Walsh, J.N., 1969. Rapid method for the determination of fluorine in silicate rocks and minerals. Anal. Chem. Acta, V. 45, p. 341-342.

Hassan, I. H. (2001): Geology, geochemistry and potentiality of radioactive mineralizations at Um Safi area, central Eastern Desert, Egypt. Ph. D. Thesis, Ain Shams Univ., Cairo, Egypt, 288 p.

Henderson, P., 1996. Rare earth elements, introduction and rivew. In: Rare earth minerals: Chemistry, origin and deposits. Edited by Jones, A.P.; Wall,

F., and Williams, C. T., The Mineralogical Society Series, p. 1-19.

Houghton, B.F., 1985. Petrology of the calc alkaline lavas of the Permian Takitimu group, Southern Newzeland, New zeal Journal Geology and Geophysics, v.28, 649-665p.

IAEA, 2003. Guidelines for radioelement mapping using gamma ray spectrometry, Data IAEA, Vienna, IAEA-TecDoc-1363.ISSN 1011–4289, Vienna.

ICRP, 2007. The 2007 Recommendations of the International Commission on Radiological Protection. ICRP Publication 103. Ann. ICRP 37 (2-4).

Irber, W., 1999. The lanthanide tetrad effect and its correlation with K/Rb, Eu/Eu*, Sr/Eu, Y/Ho, and Zr/Hf of evolving peraluminous granite suites. Geochemica et Cosmochimica Acta, Vol. 63, no. 3, p. 489-508.

Jelink, E., Soucek, J., Turdy, J., and Ulrych, J., 1989. Geochemistry and petrology of alkaline dyke rocks of the Roztoky volcanic Center, Ceske Stredohori Mountains. CSSR, Chem. Erde V.49 201-217p.

Kröner, A., 1984. Late Precambrian plate tectonic and orogeny: a need to redefine the term Pan-African. In: Kerkx, J., and Michot, J. (Eds.). Geologie Africaine-African geology, Tervuren, P. 23-28.

Kuno, H., 1959. Origin of Cenozoic Petrographic Provinces of Japan and surrounding area, Bull. Volcan, Ser. II, 20, p. 37-76.

Maniar, P.D., and Piccoli, P.M., 1989. Tectonic discrimination of granitoids. Geol. Soc. Am. Bull., No.101, p. 635-643.

Mason, B., 1966. Principles of geochemistry 3rd Ed. John Wiley, New York, 310 pp.

Middlemost, E.A.K., 1985. Magmas and Magmatic Rocks. An Introduction to Igneous Petrology. Longman Group Ltd., London, New York, 266 p

Middlemost, E.A.K., 1994. Naming Materials in the Magma/Igneous Rock System. Earth-Science Reviews, 37, 215-244. http://dx.doi.org/10.1016/0012-8252(94)90029-9

Moharem, A.F., 2002. Petrology and uranium distribution in the Um Samra - Um Bakra granitic plutons, central Eastern Desert, Egypt. Journal of the Faculty of Education, vol. 27, p. 67-90.

O'Connor, J.T., 1965. A classification of quartz - rich igneous rocks based on feldspar ratios. U.S. Geol. Surv. Prof. P. 258, P. 79-84.

Pitcher, W.S., 1993: The nature and origin of granite. Chapman & Hall, 387 pp.

Ragab, A.I., and El- Gharbawi, R.I., 1989. Wadi El- Hudi Migmatites, East of Aswan, Egypt: A geological study and some geotectonic implications for the Eastern Desert of Egypt. Elsevier Sci. Publ. B.V., Amsterdam, Precambrian Res., V. 44, p. 67 - 79.

Salman, A.B., Nossair, L.M., and El

Kholy, D.M., 1995. Contribution to the radioactivity of Gabal Homra El Gerigab, Esh El Mellaha range, north Eastern Desert, Egypt. Annals, Geol. Surv. Egypt. V. XX. P. 725-743.

Shackleton, R.M., 1986. Precambrian collision tectonics in Africa. In: Collision Tectonics. Blackwell, Oxford, P. 329-352.

Shand, S.J., 1943. Eruptive rocks, John Willey, New York. John Wiley & Sons, 444p.

Shapiro, L., and Brannock, W. W., 1962. Rapid analysis of silicate, carbonate and phosphate rocks.U.S. Geol. Surv. Bull. 1144 A, 56p.

Stern, R.J., and Hedge, C.E., 1985. Geochronology and isotopic constraints on Late Precambrian crustal evolution in the Eastern Desert of Egypt. Amer. J. Sci., V. 285, P. 97-127.

Streckeisen, A., 1976. To each plutonic rock its proper name. Earth Sci. Rev., V. 12, p. 1-33.

Taylor, S.R., 1992. Geochemistry of andesites. In: L.H. Ahrens (ed). Origin and distribution of the elements. Pergamon press, Oxford, p. 559 - 583.

Taylor, S.R., and Heier, K.S., 1965. Petrological significance of trace element variations in alkali feldspar, Proc. 2th Intern. Geol. Congr. Norden, 14, p. 47-61.

UNSCEAR, 2008. (United Nations Scientific Committee on the Effects of Atomic Radiation), Sources and effects of ionizing radiation. Report to the General Assembly, with Scientific Annexes, UNSCEAR, New York, 2008.pp. 223–242.

Villaseca, C., Barbero, L., and Herreros, V., 1998. A reexamination of the typology of peraluminous granite types in intracontinental orogenic belts. - Transactions of the Royal Society of Edinburgh: Earth Sciences, 89: 113-119.

Whalen, J.B., Currie, **K.L., and Chappell. B.W., 1987.** A-type granites: geochemical characteristics. Discrimination and petrogenesis Contrib. Mineral. Petrol. 87, p. 319-327.

الملخص العربي

المؤلفون: محمود بدران، سامح توفيق، حسين كمال الدين، وائل المعداوي، إبراهيم بديع وأمل نصر

هيئة المواد النووية

مجموعة عش الملاحة عبارة عن كتلة صخرية رفعت تكتونيا تقع في شمال الصحراء الشرقية وتعتبر الامتداد الغربي للدرع العربي-النوبي وتأخذ شكل سلسلة طويلة موازية لخليج السويس في اتجاه شمال غرب-جنوب شرق. يأخذ شكل جبل حمرة الجرجاب كتلة بيضاوية من جرانيت الفلسبار القاعدي الحديث. نشأت هذه الكتلة الجرانيتية من ماجما كلس قلوية عالية التجزئة والمحتوى الألومينى.